CONVERGENCE OF A COMPLETE FINITE-STATE INFLOW MODEL OF A ROTOR FLOW FIELD

by
Jorge A. Morillo
jam4@cec.wustl.edu
Boeing Fellow

David A. Peters
dap@mecf.wustl.edu
McDonnell Douglas Professor of Engineering

Department of Mechanical Engineering
Washington University in St. Louis
Campus Box 1185
St. Louis, MO 63130

Abstract

Dynamic inflow models have developed over the years based on the desire to develop realistic rotorcraft response tools that could be used in a design and simulation setting. The Peters-He dynamic wake model represents a mature inflow model that is used in most of the production codes and university applications. The most recent developments in inflow modeling have focused on extension of the models to include all three components of flow everywhere in the flow field, not just on the rotor disk. Extensive analysis on the frequency domain has been performed showing that this new methodology converges quickly to the exact solution in axial flow, but convergence decreases as the skew angle is increased from axial toward edgewise flow. In this paper an extensive convergence analysis is presented to determine the conditions that allow optimizing the solution obtained by this new methodology.

Introduction

Dynamic inflow models go back over 50 years in terms of their development and application. Sissingh, Ref. 1, first formulated a mathematical model that described how gradients in inflow could result from cyclic pitch changes or from fuselage pitch and roll rates. He further showed how these inflow gradients could create cyclic changes in blade angle of attack that significantly changed the actual rotor response. Curtiss and Shupe, Ref. 2, refined this idea into a lift deficiency function for rotor cyclic variations. Ormiston and Peters, Ref. 3, showed how that the formulation could be generalized into a wake model for both uniform and side-to-side variations in inflow. Comparisons with static data in hover and forward flight showed that the previous methodologies were inadequate in forward flight. Peters, generalized these concepts to the unsteady case in Ref. 4 by including apparent mass terms to account for the time delay involved in the development of the rotor flow field.

Pitt and Peters, Ref. 5, used principles of potential flow theory to show that these concepts could be developed from first principles without ad hoc assumptions on time delay or on the effects of forward flight. They obtained an unsteady flow model from potential functions that gave spectacular correlation with wind tunnel response data throughout the frequency and advance ratio range. These correlations are well documented in Ref. 6. However, despite the unquestioned success of this “Pitt-Peters” inflow model, it still remained a theory with only three inflow degrees of freedom: 1) uniform, 2) fore-to-aft, and 3) side-to-side. Although Ref. 5 investigated adding more radial functions and more harmonics (up to 8 states total possible), these ideas were not fully developed.

Later, Peters and He showed how the Pitt-Peters ideas could be truly generalized to a theory with an arbitrary number of inflow harmonics and an arbitrary number of radial shape functions per harmonic, Ref. 7. They showed how the general theory could reduce in special cases to the old Pitt-Peters model as well as to Loewy theory and Prandtl tip-loss theory. In Ref. 8, the new theory was used to correlate unsteady wind tunnel data from the NASA Langley wind tunnel for various planforms, thrust coefficients, and advance ratios. The match in both steady and unsteady distributions was excellent. Reference 9 showed how the new theory could be used even for pure hover and offered data correlation with unsteady hover test results taken in the Georgia Tech Hover Test Facility.

Once again, however, it was recognized that the new Peters-He inflow model still had areas where it was lacking such as ground effect studies. Although the original paper, Ref. 7, discussed an approximate

Presented at the 28th European Rotorcraft Forum, Bristol, England, September 17-20, 2002.

way to estimate the effect of steady ground effect on the uniform flow, there existed no generalized way to include dynamic ground, tilted ground, partial ground, or to find the entire flow field in the presence of normal ground effect. Prasad et al, Ref. 10, showed that uniform ground could be simulated by an image rotor below the ground plane. However, this methodology did not apply in hover. Xin, et al, Ref. 11 showed that the ground could also be modeled by a source disk at the ground plane, itself. This could then be used in hover as well as for inclined ground and partial ground. Further work, Ref. 12, showed how quasi-steady effects could be added. A summary of the various models can be found in Ref. 13. Once again, the formulation remains in the context of classical inflow theories but with added states included for the ground source.

However, in the ground effect work, it is necessary to find not just the normal flow at the disk, but all three components of flow off of the disk as well. Peters and Morillo, Ref. 14, presented a consistent methodology for computing all three components of the flow in axial flow, both on and off of the rotor disk within the context of a finite-state model. The model is formulated in a manner fairly similar to previous work (in that the potential functions in ellipsoidal coordinates are used). However, in contrast with the previous work, the states represent velocity potentials rather than individual flow components. In addition, all potential functions are considered (not just the ones that have a pressure discontinuity across the disk); and the derivation of the equation coefficients is done in a more consistent and rigorous manner than in the earlier derivations. The result is a simpler derivation and a more complete inflow theory for the velocity both off and on the disk. Previous dynamic inflow models in axial flow are shown to be special cases of the new model when off-disk coupling is neglected. This new methodology based on a Galerkin approach provides the exact solution on as well as off the disk for the axial velocity component in axial flow.

Later, Morillo and Peters, Ref. 15, extended the model to analyze skewed flows. As the wake skew angle is varied from axial flow toward edgewise flow, the new model, continues to converge to the true solution at all wake skew angles, but it shows a trend of decreasing rate of convergence on the downstream side as the skew angle approaches edgewise flow.

This paper will present a study of the nature of the convergence of this new methodology and ways to improve it.

Mathematical Basis

The following is the mathematical basis for the new, complete inflow model for skewed flow developed in Ref. 15. First, the pressure and velocities functions are written as gradients of the pressure and velocity potentials in ellipsoidal coordinates (ν, η, $\overline{\psi}$), Ref. 16, as shown below:

$$P = -\sum_{m=0}^{\infty}\sum_{n=m+1}^{\infty}\left(\tau_n^{mc}\Phi_n^{mc} + \tau_n^{ms}\Phi_n^{ms}\right) \tag{1}$$

$$\vec{v} = \sum_{m=0}^{\infty}\sum_{n=m}^{\infty}\left(\hat{a}_n^m\vec{\nabla}\Psi_n^{mc} + \hat{b}_n^m\vec{\nabla}\Psi_n^{ms}\right) \tag{2}$$

where

$$\Psi_n^{mc} = \int_{\xi}^{\infty}\Phi_n^{mc}d\xi \qquad \Psi_n^{ms} = \int_{\xi}^{\infty}\Phi_n^{ms}d\xi \tag{3}$$

$$\Phi_n^{mc}(\nu,\eta,\overline{\psi}) = \overline{P}_n^m(\nu)\overline{Q}_n^m(i\eta)cos(m\overline{\psi}) \tag{4}$$

$$\Phi_n^{ms}(\nu,\eta,\overline{\psi}) = \overline{P}_n^m(\nu)\overline{Q}_n^m(i\eta)sin(m\overline{\psi}) \tag{5}$$

and $\overline{P}_n^m(\nu)$ and $\overline{Q}_n^m(i\eta)$ are normalized associated Legendre functions of first and second kind, Ref. 16.

The equations of motion in this new formulation have the following structure where, for convenience, only the cosine terms are shown

$$\left[\tilde{L}^c\right]\left\{\overset{*}{\hat{a}}_n^m\right\} + \left[D^c\right]\left\{\hat{a}_n^m\right\} = \left[D^c\right]\left\{\tau_n^{mc}\right\} \tag{6}$$

Each one of the elements of the $\tilde{L}^c$ and D^c matrices are known in closed form. The expressions are shown in the Appendix.

Equation (6) is valid for any skew angle χ, which appears in the equation in the expressions for the wake influence coefficient matrix $\tilde{L}^c$. This equation can be further partitioned into two row-groups and two column-groups such that *m+n* (or *j+r*) is odd and *m+n* (or *j+r*) is even. These matrices are organized in the following way

$$\begin{bmatrix} \begin{bmatrix} j+r=odd, \\ n+m=odd \end{bmatrix} & \begin{bmatrix} j+r=odd, \\ n+m=even \end{bmatrix} \\ \begin{bmatrix} j+r=even, \\ n+m=odd \end{bmatrix} & \begin{bmatrix} j+r=even, \\ n+m=even \end{bmatrix} \end{bmatrix} \begin{Bmatrix} \{n+m=odd\} \\ \{n+m=even\} \end{Bmatrix} \tag{7}$$

If Eq. (6) is organized as suggested in Eq. (7), it can be partitioned as

$$\begin{bmatrix} \left[\tilde{L}\right]_{o,o} & \left[\tilde{L}\right]_{o,e} \\ \left[\tilde{L}\right]_{e,o} & \left[\tilde{L}\right]_{e,e} \end{bmatrix} \begin{Bmatrix} \left\{\overset{*}{\hat{a}}_n^m\right\}_o \\ \left\{\overset{*}{\hat{a}}_n^m\right\}_e \end{Bmatrix} + \begin{bmatrix} [D]_{o,o} & [D]_{o,e} \\ [D]_{e,o} & [D]_{e,e} \end{bmatrix} \begin{Bmatrix} \left\{\hat{a}_n^m\right\}_o \\ \left\{\hat{a}_n^m\right\}_e \end{Bmatrix} = \begin{bmatrix} [D]_{o,o} & [D]_{o,e} \\ [D]_{e,o} & [D]_{e,e} \end{bmatrix} \begin{Bmatrix} \left\{\tau_n^m\right\}_o \\ \left\{\tau_n^m\right\}_e \end{Bmatrix} \tag{8}$$

From Eqs. (2) and (3), it is seen that, to compute the velocity field, it is required to compute the velocity potentials, Ψ_n^m, by a numerical integration.

To avoid numerical integration and in order to be able to express the velocity potentials in terms of potentials known everywhere in the flow field, a change of variable from $\hat{a}_n^m$ to a_n^m is introduced

$$\left\{\hat{a}_n^m\right\}^T\left\{\Psi_n^{mc}\right\}=\left\{a_n^{mc}\right\}^T\left\{\sigma_n^m\Phi_{n+1}^{mc}+\varsigma_n^m\Phi_{n-1}^{mc}\right\} \tag{9}$$

The constants σ_n^m and ς_n^m are chosen such that the new velocity potential will give no singularities when gradients of it are taken.

$$\sigma_n^m=\frac{1}{K_n^m\sqrt{(2n+1)(2n+3)\left((n+1)^2-m^2\right)}} \tag{10}$$

$$\varsigma_n^m=\frac{1}{K_n^m\sqrt{\left(4n^2-1\right)\left(n^2-m^2\right)}};n\neq m \tag{11}$$

where

$$K_n^m=\left(\frac{\pi}{2}\right)^{(-1)^{n+m}}H_n^m \tag{12}$$

$$H_n^m=\frac{(n+m-1)!!(n-m-1)!!}{(n+m)!!(n-m)!!} \tag{13}$$

If Eq. (9) is substituted into Eq. (6), the set of ordinary differential equations for the velocity coefficients in terms of the pressure coefficients for skewed flow becomes,

$$\left[M^c\right]\left\{\overset{*}{a}_n^m\right\}+\left[D^c\right]\left[\tilde{L}^c\right]^{-1}\left[M^c\right]\left\{a_n^m\right\}=\left[D^c\right]\left\{\tau_n^{mc}\right\} \tag{14}$$

From the results obtained thus far in Refs. 14 and 15, several important conclusions work together to define the development of this paper. First, comparisons for the on-disk axial velocity component in axial flow computed by the old Peters-He model, by the new model, and by exact solutions show that the new model converges to the true solution and that the old model does not. Although the differences are mainly seen for the lower harmonics and for radial distributions at intermediate frequencies, they are definitely significant. For off-disk flow, only predicted by the new model, convergence is also excellent.

Second, as the wake skew angle is varied from axial flow toward edgewise flow, the Peters-He model converges more quickly than the new model for flow on the disk. (Recall that that model does not give flow anywhere else). By the time that purely edgewise flow is encountered, the old model is virtually exact (except at very high frequencies). The new model, on the other hand, while continuing to converge to the true solution at all wake skew angles, shows a trend of decreasing rate of convergence on the downstream side as the skew angle approaches edgewise flow. Although it is easy to see theoretically why perfectly edgewise flow cannot converge downstream, one would still expect better on-disk convergence given that the old Peters-He model gives excellent on-disk results even at edgewise flow.

This focuses our attention on the study of the nature of the convergence and ways to improve it. It is known that the choice of basis functions can have a profound effect on convergence, Refs. 17 and 18. To analyze the convergence of this new methodology, the inflow model with an original odd-even partitioning will be considered with truncation of even terms. This model will be studied since it is the most basic of our derivations and seems to have a good convergence in the previous results. Additionally, truncation of even-numbered terms will help with the conditioning problem of $\tilde{L}^c$, as it was indicated in Ref. 15.

Results

The convergence of the results will be determined by comparing the exact results obtained with the convolution approach, Ref. 16, with the results obtained with the Galerkin approach. The error norm, *E*, between two distributions v_1 and v_2 is defined as

$$(E)^2=\frac{\int_{r=r_o}^{r_f}(v_1-v_2)^2\sqrt{1-r^2}\,rdr}{\int_{r=r_o}^{r_f}v_1^2\sqrt{1-r^2}\,rdr} \tag{15}$$

For the Galerkin approach, two errors can be defined. One for the on-disk region (r_o=*-1;* r_f=*1*), and one for the on/off-disk region (r_o=*-2;* r_f=*2*) at an azimuth angle $\bar{\psi}$. The error norm will be plotted, so that an over-all feeling can be obtained for the effect of neglecting inflow modes that are zero on the disk (*n+m=even*).

In order to determine the number of even terms included in the solution, the table method will be used, Ref. 16. In this methodology, the number of harmonics, *m*, is equal the highest dynamic frequency of interest. For the choice of the number of radial shape functions to be used for each harmonic, a mathematically consistent hierarchy was set up to determine the number of radial shape functions for each harmonics, *m* in order to have radial terms up to a given power of *r*. Based on this methodology, the number of terms, odd or even, included in the solution could be specified in four different ways: 1) by indicating the number of harmonics, *m*, 2) by indicating the number for the highest power of *r*; 3) by indicating the number of terms for the zeroth harmonic; or 4) by indicating the index of the highest subscript, *n,* of the Φ_n^m terms. All of these possibilities are related by the following expressions:

$$highest\ power\ of\ r = m \tag{16}$$

$$terms@zeroth\ harmonics = Int\left(\frac{highest\ power\ of\ r}{2}\right) + 1 \tag{17}$$

$$Index\ of\ highest\ subscripts = \begin{Bmatrix} m+1; odd\ terms \\ m+2; even\ terms \end{Bmatrix} \tag{18}$$

where *Int(x)* is a function that rounds the elements of *x* to the nearest integer towards zero.

In this paper, two different sizes for the submatrix with *n+m=odd* and *j+r=odd* will be considered, one with *m=10*, and one with *m=20*. The number of terms in the solution will be identified by indicating the index of the highest subscripts, *n*, of the Φ_n^m terms. Thus, unless otherwise is indicated, an index indicates the highest value of *n* for the Φ_n^m terms.

For each one of the cases considered in this paper, the index for the even terms is varied from zero to a number equivalent to the one included for the odd terms. With zero as the index for the even terms, the model is equivalent to the Peters-He model.

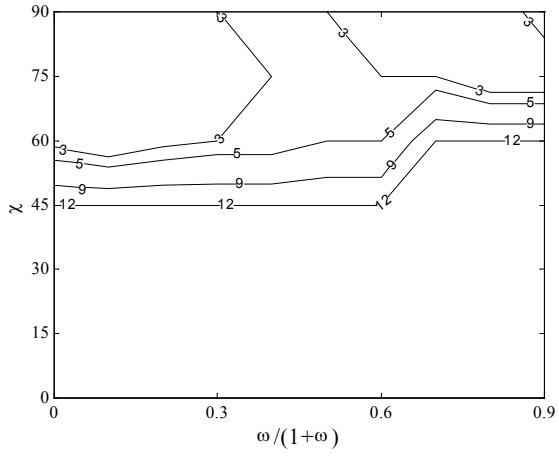

(a)

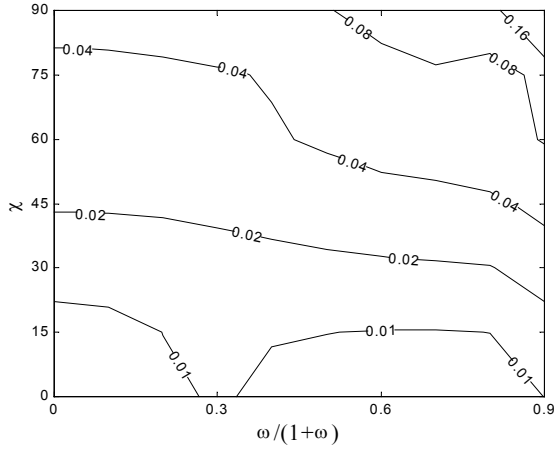

(b)

Fig.1(a) Index of highest subscript, $P = \Phi_1^0$, m_{odd}=10; (b) $E = (E_{min})_{on-disk}$.

Figures 1(a) through 4(a) show contour plots for the index for the even terms required in the Galerkin approach solution in order to minimize the error in the axial component of the induced velocity in the on-disk region as a function of the skew angle and the reduced frequency. In all the cases, the velocities are computed at the rotor disk plane (*z=0*), *s*, and for *y=0*. Figures 1(b) through 4(b) show contour plots for the minimum error on the disk area also as a function of the skew angle and the reduced frequency. Note that the reduced frequency is plotted as $\omega/(\omega+1)$. With this representation, the complete range of frequency from 0 up to ∞ could be seen. In this paper, the reduced frequency considered goes from 0 up to 9. For typical problems of rotorcraft maneuverings, the reduced frequency (not per/rev frequency) is less than 0.5, which gives $\omega/(\omega+1)$<0.333 and for typical propeller blade-passage frequencies $\omega/(\omega+1)$>0.6. Thus, unless otherwise mentioned, when referring to the frequency range, rotorcraft region implies $\omega/(\omega+1) \leq 0.3$ and propeller blade-passage region indicates $\omega/(\omega+1) \geq 0.6$.

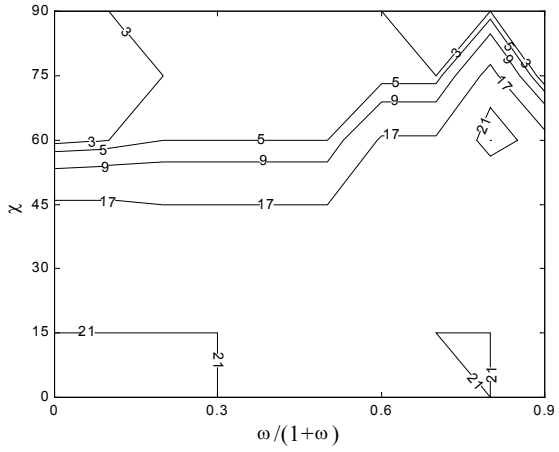

(a)

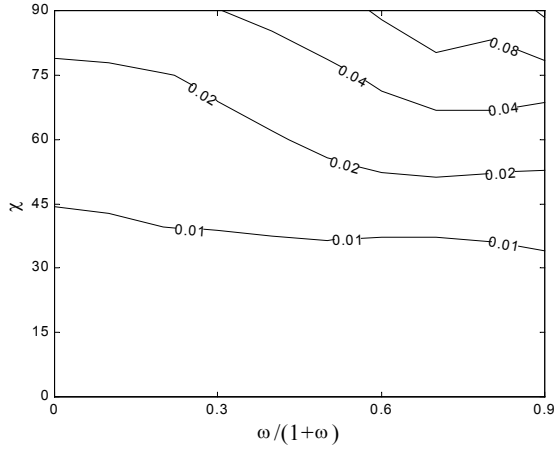

(b)

Fig.2(a) Index of highest subscript, $P = \Phi_1^0$, m_{odd}=20; (b) $E = (E_{min})_{on-disk}$.

Figures 1 and 2 are for the first collective pressure input Φ_1^0 with two different number of harmonics for the odd terms included in the solution, 10 and 20, respectively. For Fig.1 the maximum possible number for the index for the even terms to be included is 12, and the minimum is *0* (Peters-He model). Figure 1 shows that for the complete frequency range plotted, $\omega/(\omega+1) \le 0.9$, and $\chi \le 45^o$ the minimum error is provided by the original matrix without any truncation. In that region, the solution provided for the Galerkin approach is exact at $\chi = 0^o$ (axial flow), and the error is less than 4% for a skew angle of $\chi \le 45^o$. On the other hand, for a very steep skew angle, $\chi \ge 75^o$, the minimum error is provided by a solution with at most 3 as the index (i.e., at most m_{even}=*1*) The minimum error goes from 4%, for rotorcraft frequencies, up to 16%, for propeller blade passage frequencies. The maximum possible number for the index for the even terms for Fig.2 is 22. In this figure, for $\chi \le 45^o$ the index for the even terms that produces the minimum error never reaches the possible maximum number; and at $\chi \ge 75^o$, and higher frequencies $\omega/(\omega+1) \ge 0.7$, the best solution is provided with a relatively large number of even terms in the solution. The minimum error for $\chi \le 45^o$ is about 1%, and for $\chi \ge 75^o$ goes from 2% up to 16%. Comparisons between Figures 1(b) and 2(b) show that as the number of harmonics for the odd terms is increased (i.e., number of odd terms), the error produced by the Galerkin approach on the on-disk area for a given frequency and skew angle is reduced.

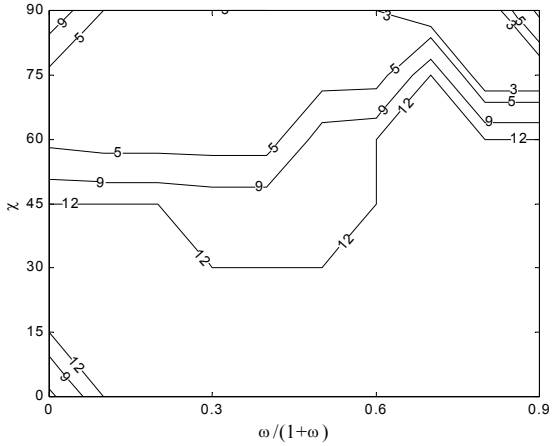

(a)

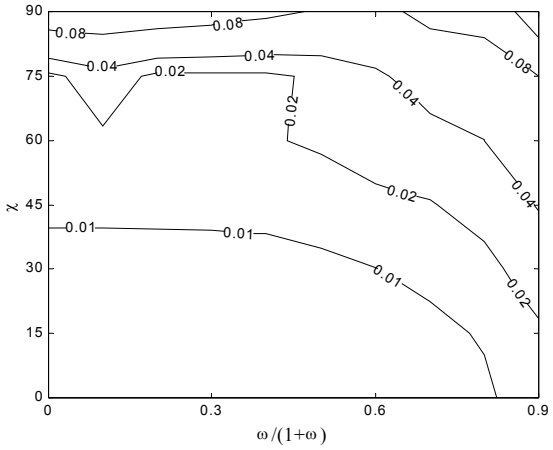

(b)

Fig.3(a) Index of highest subscript, $P = \Phi_2^1$, m_{odd}=10; (b) $E = (E_{min})_{on-disk}$.

Figures 3 and 4 are for the first cyclic pressure input Φ_2^1. Figure 3 is for 10 as the number of harmonics in the odd terms included in the solution. In Fig.3(a) it is observed that the optimum number of even terms to be included in the solution (to minimize the error) depends on the skew angle and on the frequency. For skew angles $\chi \le 45^o$ it is required to include the maximum index for the even terms to minimized the error either for $0 \le \omega/(\omega+1) \le 0.2$ and $0.6 \le \omega/(\omega+1) \le 0.9$. For the intermediate values, the best solution is provided is the even matrix is truncated (i.e. $9 \le index \le 12$). This behavior is different than the one observed for the pressure collective inputs in which for $\chi \le 45^o$ the best solution is provided by including the maximum amount of even terms independently of the frequency. It is also observed that for skew angles $\chi \ge 60^o$ the number of terms that produces the minimum error is sensitive to frequency. For rotorcraft frequencies, a low index value for the even terms is needed (only *5* out of *12*), but for intermediate and propeller blade-passage frequencies, the index needs to be increased considerably.

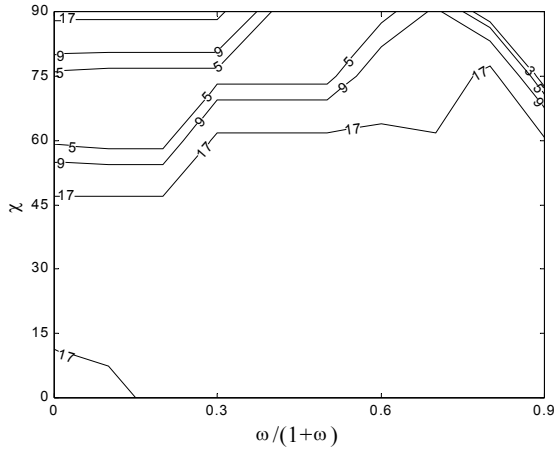

(a)

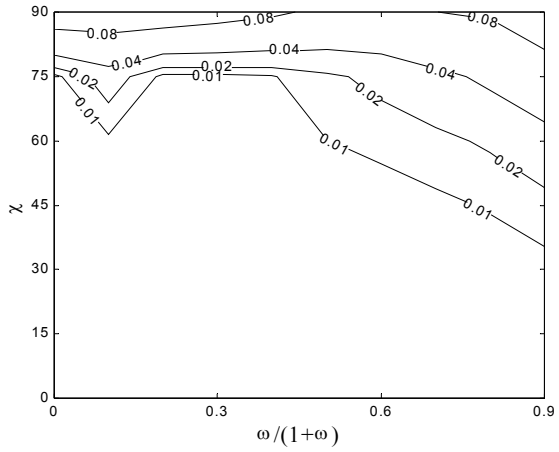

(b)

Fig.4(a) Index of highest subscript, $P = \Phi_2^1$, m_{odd}=20; (b) $E = (E_{min})_{on-disk}$.

From Fig.3(b), the error in the on-disk region for $\chi \le 45^o$ is less than 2 % for rotorcraft and intermediate frequencies, and for propeller blade-passage frequencies it can go up to 4%. As the skew angle and the frequency are increased, the error increases. For edgewise flow, low and intermediate frequencies, the error is 8%, and for high frequencies, it increases above 16%.

If the number of harmonics for the odd terms is increased to 20, Fig.4, it is observed that for $\chi \le 45^o$, the index for the even terms is 17 for any value of frequency. For skew angles $45^o \le \chi \le 75^o$, the optimum solution is sensitive to the frequency. For steep skew angles $\chi \ge 75^o$, the solution depends on the frequency and on the skew angle. For low frequencies, despite the behavior observed for the collective pressure inputs as the skew angle increases, the index also increases. For frequencies $0.3 \le \omega/(\omega+1) \le 0.9$, the behavior is opposite, the steeper the skew angle, the lower the index for the even terms. For this region, and for intermediate frequencies, an index of 5 is required, but for propeller blade-passage frequencies, one could need an index as high as 17. On Fig.4(b), for skew angles $\chi \le 75^o$, the error is sensitive to frequency. For $0 \le \omega/(\omega+1) \le 0.4$, the error is about 2% for any frequency, but for $0.4 \le \omega/(\omega+1) \le 0.9$, the error can go from 2% up to 6%. For $\chi \ge 75^o$, the relation between the error and the frequency is less marked, until a point in which edgewise flow is encountered and the error is about 8% for any value of frequency.

Based on the results presented in Figs. 1 through 4, it is possible to indicate that, to minimize the error for low skew angles (i.e. $\chi \le 45^o$), a high value for the index of the even terms is required. It is also observed from these figures that the Galerkin approach provides an exact solution for axial flow, $\chi = 0^o$, for the entire range of frequencies.

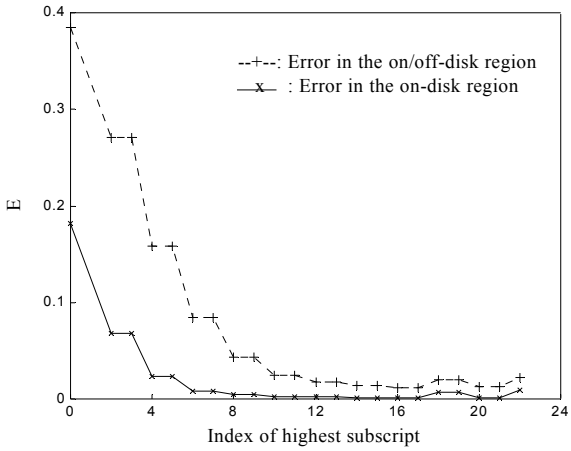

Fig.5 Error, ω=2.3, $P = \Phi_1^0$, $\chi = 0^o$, m_{odd}=20.

Figure 5 shows the error norm in the axial component of induced velocity in axial flow at ω=2.3 for a pressure distribution Φ_1^0 as a function of the highest subscript index for the even terms that are included in the velocity expansions. The number of harmonics in the odd terms is 20. This number of harmonics will be kept in all the remaining figures. The figure shows that, by adding to the Peters-He model one even term (i.e., 2 as the index), the error norm is reduced from its original value of 18.8% down to 6.8%. If the index is increased up to 6, the error is only 1%. The minimum error is obtained when 16 is the index for the even terms (0.14%). It is also shown the error in the solution on the entire rotor disk plane both on and off-disk ($-2 \le x \le 2$). It will be called on/off-disk error. It goes from 38.5% when no even term is included down to a minimum of 1.2% when even terms with 16 as the index are included. Both errors decay essentially monotonically as the index of the even terms is increased. Note that only every other index occurs in the even terms.

Figure 6 shows similar results for Φ_2^1 at ω=7.3. In this case, only even terms with 7 as the index are required to reduce the on-disk error to about 1%. The

on/off-error goes from 30% up to 0.7% when terms with index of 17 are included.

The frequencies analyzed for the axial flow cases, Figs. 5 and 6, are the frequencies at which the Peters-He model introduced the maximum error for these pressure distributions, Ref. 14.

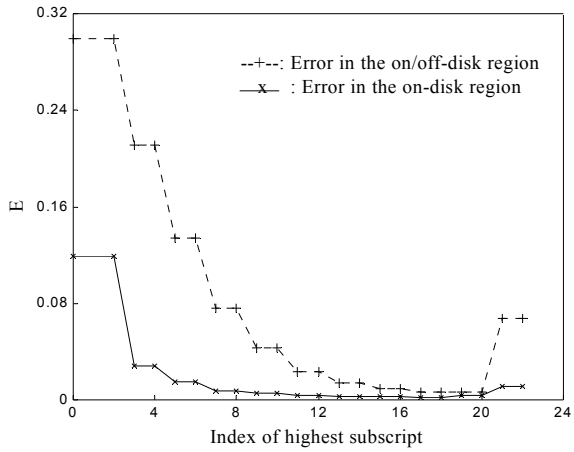

Fig.6 Error, ω=7.3, $P = \Phi_2^1$, χ=0°, m_{odd}=20.

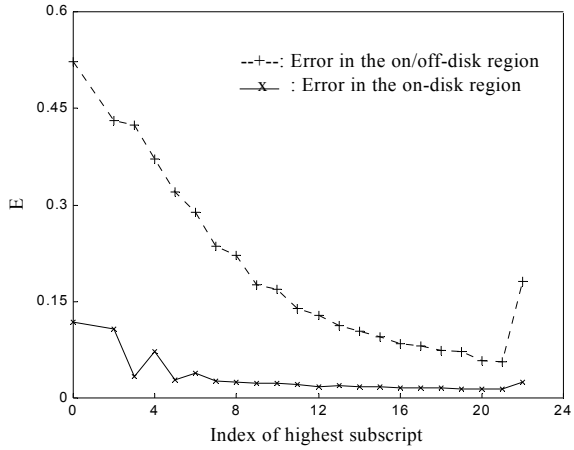

Fig.7 Error, ω=4.0, $P = \Phi_1^0$, χ=45°, m_{odd}=20.

It is convenient to analyze the behavior of the convergence of the on-disk solution for steeper skew angles (i.e. $\chi \geq 45^o$) to see if it is possible to find a pattern to describe the index for the even terms needed in the approximate solution, as it was done for $\chi \leq 45^o$.

In Figs. 7 through 12, three different skew angles are considered. Figures 7 and 8 are for $\chi=45^o$, Figs. 9 and 10 for $\chi=75^o$, and Figs. 11 and 12 for perfectly edgewise flow, $\chi=90^o$.

Figure 7 shows the on-disk and on/off-disk errors when the input is the Φ_1^0 at a frequency ω=4. In this case, the minimum error, 1.33%, is obtained when even terms with index up to 21 are included in the solution. It is important to notice that the on-disk error when no even term is included is 11.77%, Ref. 16, lower than its value for axial flow. It indicates that the error introduced by the Peters-He model decreases as the skew angle increases. Another observation about the convergence of the on-disk error is that instead of decreasing monotonically as it does for axial flow, its convergence is slower when few even terms are considered (i.e. terms with index less than 8) and after that it decreases until it reaches a minimum when 21 is the index for the even terms considered in the solution. After this point, the on-disk error starts to diverge, even thought the $\tilde{L}^c$ matrix still well-conditioned, Ref. 16. On the other hand, the on/off-disk error exhibits behavior similar to axial flow. The error decreases until it reaches a point in which starts to diverge. The minimum on/off-disk error, 5.63%, increases as the skew angle is increased. This is due to the error obtained in the velocity in the off-disk trailing edge area of the rotor disk plane.

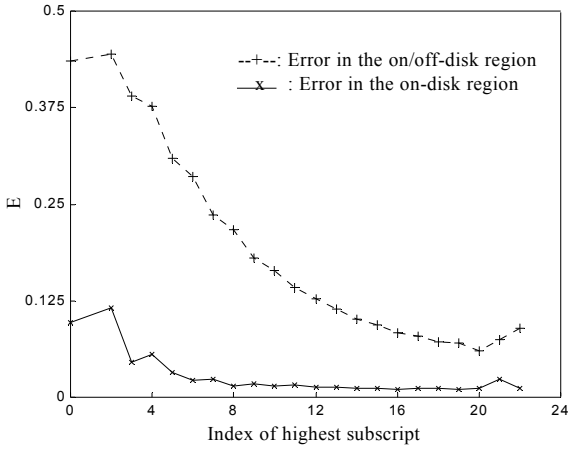

Fig.8 Error, ω=4.0, $P = \Phi_2^1$, χ=45°, m_{odd}=20.

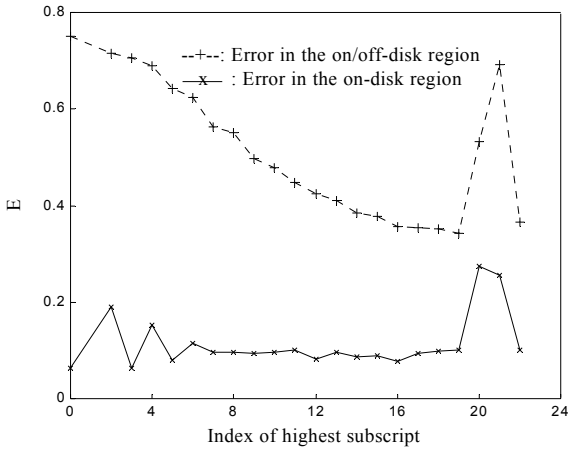

Fig.9 Error, ω=4.0, $P = \Phi_1^0$, χ=75°, m_{odd}=20.

Figure 8 shows the on and on/off-disk errors for a first cyclic pressure distribution Φ_2^1 at a frequency ω=4.0. The on-disk error increases from 9.74% to 11.54% when 1 even term is included (index equal to 2) and then decreases up to 1.06% when 18 is the index for the even terms included. It is also observed

that at this frequency the error does not evidently diverge as it does on the previous figures. The on/off error also increases when only 1 even term is included, and then decreases as the index for the even terms increases up to 20. The minimum error is *6*%.

Figure 9 is for the first collective pressure input Φ_1^0 at χ=*75*^{o} and ω=*4.0*. The on-disk error does not monotonic decrease as the number of even terms is increased, instead it converges slowly. In this case, if no even term is included in the solution (Peters-He model), the error is *6.27*%, if the index for the even terms is increased to 3, the error is 6.35%, and if no truncation is done on the even terms, the error is 7.3%. Thus, the error with a small number of even terms included in the solution is lower than the one obtained when a large number of even terms are included. For the same pressure input and frequency but at a skew angle χ=*45*^{o}, the error introduced by the Peters-He model is *11.7*%, Fig. 7. Thus, the Peters-He model becomes more accurate as the skew angle is increased. On the other hand, the minimum on-disk error introduced by the Galerkin approach at χ=*75*^{o} is *7.8*% which is higher compared with *1.33*% obtained for χ=*45*^{o}. Therefore, the Galerkin approach converges more slowly as the skew angle is increased. For the on/off-disk solution, it is observed that the error decays as the index for the even terms is increased up to 19 (75.2% for the Peters-He model and *34.3*% for 19 as the index for the even terms included in the solution), after that, the error increases as the number of even terms increases. If Fig. 9 is compared with the one for χ=*45*^{o} (Fig.6), it is noted that the minimum error that the methodology achieves for the on/off-disk solution is much higher than before. Also, the index for the even terms that produces the minimum error in the on/off-disk region reduces from *21* to 1*9*. Again, the increase in the on/off-disk error is due to the loss of accuracy in the solution on the trailing off-disk region.

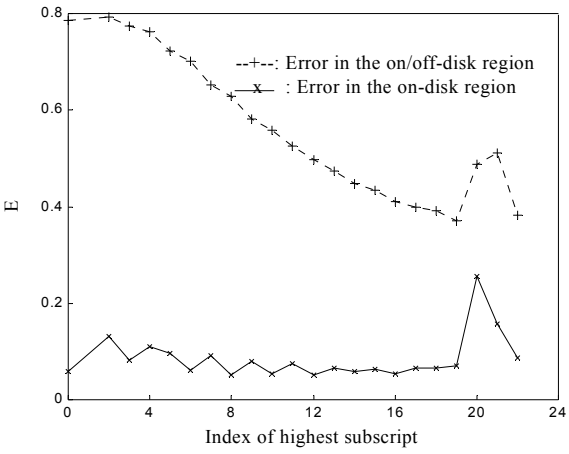

Fig.10 Error, ω=4.0, $P=\Phi_2^1$, χ=75^o, m_{odd}=20.

Figure 10 is for the first cyclic pressure distribution Φ_2^1 and ω=*4.0*. For the on-disk region, the minimum error, *5.06*%, is obtained with 8 as the index for the even terms included in the solution. This error is similar to the one obtained with no even terms and with 12 as the index, *5.78*% and *5.87*%, respectively. If this figure is compared with the one for the same pressure input and frequency, but for a skew angle χ=*45*^{o}, it is observed that the convergence is slower and that the Peters-He model becomes more accurate while the Galerkin methodology lose accuracy. For the on/off-disk region, the error reduces from *78.56*% up to *36.98*% when 1*9* is the index.

The pressure input in Fig.11 is the first collective pressure Φ_1^0, but perfectly edgewise flow is analyzed. The convergence of the error in the on-disk region is again slow, and the minimum error is achieved with the index is 3 for the even term, 9.9%. The error introduced by the Peters-He model is higher (11.84%) as compared with the results obtained for χ=*75*^{o}, and similar loss of accuracy is observed on the Galerkin methodology. For the on/off-disk region, the best solution is also obtained with 3 as the index.

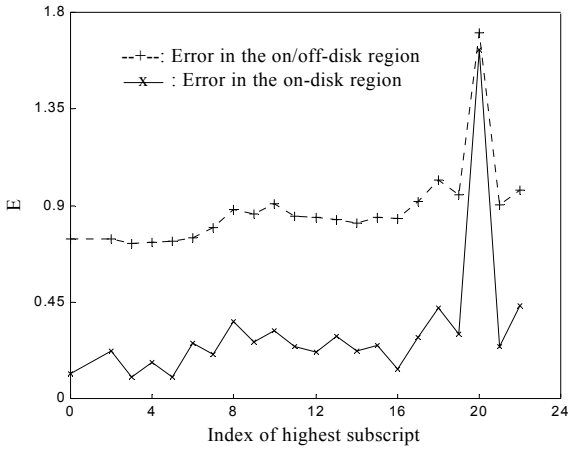

Fig.11 Error, ω=4.0, $P=\Phi_1^0$, χ=90^o, m_{odd}=20.

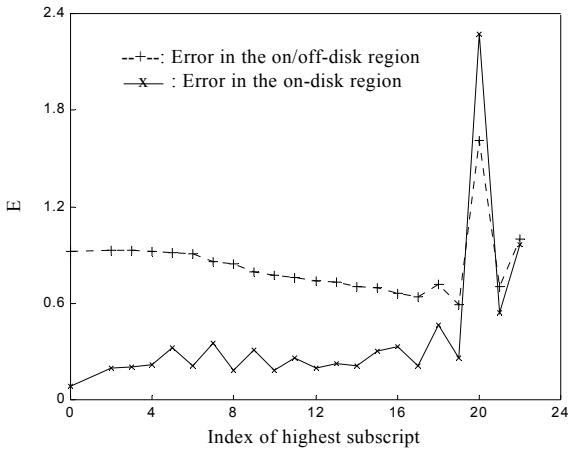

Fig.12 Error, ω=4.0, $P=\Phi_2^1$, χ=90^o, m_{odd}=20.

On Fig.12 (first cyclic pressure Φ_2^1, χ=90°, and ω=4.0), the minimum error in the on-disk region is produced by the Peters-He model, 8.44%. Again, this value is higher if compared with the one obtained for χ=75°. For the on/off-disk region, the error reduces from 92.05% to 58.85% when an even term with an index of 19 is included. Note that for this number of even terms, the on-disk error increases from 8.44% to 25.7%.

The results shown on Figs 5 through 12, show that for steep skew angles, the minimum error in the on-disk solution for the axial component of the induced velocity is obtained by including in the approximate solution a small number of even terms. On the other hand, in all these figures, it is shown that including a small number of even terms would significantly affect the on/off-disk error. Thus, if the off-disk value of the induced velocity is needed at the rotor disk plane, it is convenient to include a large number of even terms

Based on these results, the following expression is suggested to obtain the index for the even terms to be included to minimize the error in the on-disk solution.

$$\frac{even\ terms}{odd\ terms} = \frac{3}{2}\sqrt{\cos(\chi)}; \quad 0^o \le \chi \le 90^o \tag{19}$$

If it is desired to minimize the error in the on/off-disk region

$$\frac{even\ terms}{odd\ terms} = .75; \quad 0^o \le \chi \le 90^o \tag{20}$$

Analysis with other pressure as well as mass-source inputs has been performed in Ref. 16, which validates equations (19) and (20) for any input, skew angle and reduced frequency.

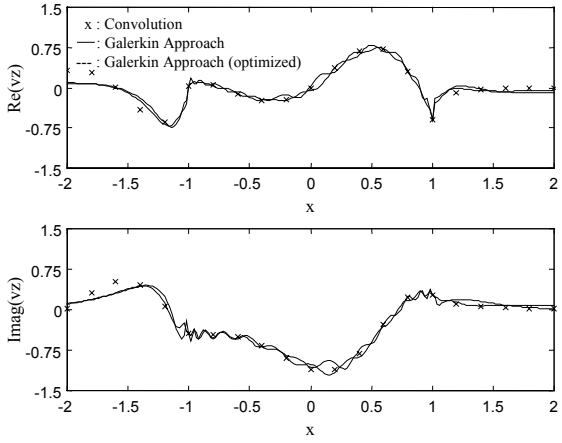

Fig.13 Frequency response, ω=4.0, $P = \Phi_1^0$, χ=75°, z=0.

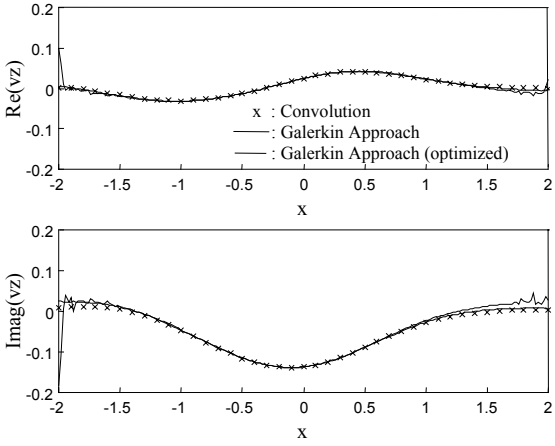

Fig.14 Frequency response, ω=4.0, $P = \Phi_1^0$, χ=75°, z=-1.

Figures 13 and 14 compare the frequency response for the first collective pressure distribution Φ_1^0 for two different number of even terms included in the solution, one is with an equal number of odd and even terms and one with the number of even terms indicated by equation (20); and at two different locations, one is on the rotor disk plane, Fig. 13, and one is a distance equal of one radius above the rotor disk plane, Fig. 14. In both figures the frequency is ω=4.0, and the skew angle is χ=75°.

In Fig. 13, although the optimized solution converges faster than the one with equal number of odd and even terms, the optimized on-disk response shows some oscillations about the exact, in-phase as well as out-of-phase. The convergence in the leading off-disk region (although similar) is slightly faster in the optimized solution especially in the in-phase response. In the trailing off-disk region, both solutions converge to the exact one up to about x=-1.5.

In Fig. 14, it is observed a better agreement between the Galerkin solution and the exact solution in the region located above the on-disk area. The improvement in the solution is also observed in the region above the off-disk trailing and leading area. Even thought the improvement introduced in the solution, it is observed that the optimized solution converges to the exact solution on the complete range of x values, while the solution with similar number of odd and even terms seems to deteriorate after x=±1.5. This deterioration has also been observed in rotor disk plane solutions at distance of 3 times the rotor radius.[16] This may be due to error is the computation of $\overline{Q}_n^m(i\eta)$ [16] for large η.

Summary and Conclusions

An extensive convergence analysis is performed with solutions with up to 20 harmonics for the odd and even terms, and it is concluded that the number of odd

and even terms to be included in the solution depends on the exactness required, the skew angle considered, and the desire to optimize the on-disk or the on/off velocity profile.

The index for the even terms required in the solution to minimize the error in the on-disk area is expressed as a function of the skew angle. If it is desired to optimize the on/off velocity profile, the ratio of the indexes for even terms over odd terms is a constant equal to 0.75.

If the optimum values of even terms are included in the solution for 20 as the harmonic for the odd terms, it is observed that the Galerkin approach is exact in axial flow, and that it introduces a maximum error of about 16% at perfectly edgewise flow and high frequencies. For the rotorcraft range of value ($\chi \leq 75^o$ and $\omega/(1+\omega) \leq 0.3$) the error is always less than 4% for any pressure or mass-source distribution.

Acknowledgement

This work was sponsored by the Boeing Washington University Partnership Program, and by the Army Research Office (Technical Monitor: Tom Doligalski).

References

[1]Sissingh, G.J., "The Effect of Induced Velocity Variation on Helicopter Damping in Pitch or Roll," Aeronautical Research Council (Great Britain), A.R.C. Technical Report C.P. No. 101 (14, 757), 1952.

[2]Curtiss, H.C., Jr., and Shupe, N.K., "A Stability and Control Theory for Hingeless Rotors," Proceedings of the 27th Annual National Forum of the American Helicopter Society, Washington, D.C., May 1971.

[3]Peters, David A. and Ormiston, R.A., "Hingeless Helicopter Rotor Response with Nonuniform Inflow and Elastic Blade Bending," *Journal of Aircraft*, Vol. 9, No. 10, October 1972, pp. 730-736.

[4]Peters, David A., "Hingeless Rotor Frequency Response with Unsteady, Inflow," Proceedings of the American Helicopter Society Dynamics Specialists' Meeting, Ames Research Center, NASA SP-352, February 1974.

[5]Pitt, D. M. and Peters, David A., "Theoretical Prediction of Dynamic Inflow Derivatives," *Vertica*, Vol. 5, No. 1, March 1981, pp. 21-34.

[6]Gaonkar, Gopal H. and Peters, David A., "Review of Dynamic Inflow Modeling for Rotorcraft Flight Dynamics," *Vertica*, Vol 12, No. 3, 1988,pp. 213-242.

[7]Peters, David A., He, Chengjian, and Boyd, David Doug, "A Finite-State Induced-Flow Model for Rotors in Hover and Forward Flight," *Journal of American Helicopter Society,* Vol. 34, No. 4, October 1989, pp. 5-17.

[8]Peters, David A. and He, C-J, "Correlation of Measured Induced Velocities with a Finite-State Wake Model," *Journal of American Helicopter Society*, Vol. 36, No. 3 July 1991, pp. 59-70.

[9]Su, A., Yoo, Kyung M., and Peters, David A., "Extension and Validation of an Unsteady Wake Model for Rotors," *Journal of Aircraft*, Vol. 29, No. 3, May - June, 1992, pp. 374-383.

[10]Prasad, J. V. R., Xin, Hong, Peters, D. A., Nagashima, T. and Iboshi, N., "Development and Validation of a Finite State In-Ground Effect Inflow Model for Lifting Rotors," Proceedings of the AHS Technical Specialists' Meeting for Rotorcraft Acoustics and Aerodynamics, Stratford, Connecticut, October 28-30, 1997.

[11]Xin, et al, "Ground Effect Aerodynamics of Lifting Rotors Hovering above Inclined Ground Plane," presented at the AIAA Applied Aerodynamics and CFD Conference, Norfolk, Virginia, June 28 – July 1, 1999, AIAA-99-3223.

[12]Xin, Hong, Prasad, J. V. R., Peters, D. A., "Dynamic Inflow Modeling for Simulation of a Helicopter Operating in Ground Effect," presented at the AIAA Modeling and Simulation Technology Conference, Portland, Oregon, August 9 – 11, 1999, AIAA-99-4114.

[13]Xin, H., Prasad, J. V. R., Peters, D., Ibushi, N. and Nagashima, T., "Correlation of Experimental Measurements with a Finite-State Ground Effect Model," Proceedings of the 56th Annual National Forum of the American Helicopter Society, Virginia Beach, May 1-4, 2000, pp. 421–430.

[14]Peters, David A. and Morillo, Jorge A., "Towards a Complete Dynamic Wake Model in Axial Flow," Proceedings of the American Helicopter Society Aeromechanics Specialists' Meeting, Atlanta, Georgia, November 13–14, 2000.

[15]Morillo, Jorge A. and Peters David A., "Extension of Dynamic Inflow Models to Include Mass Injection and Off-Disk Flow," Proceedings of the 40th AIAA Aerospace Sciences Meeting & Exhibit, Paper No. AIAA-2002-0716. Reno, Nevada, January 14-17, 2002.

[16]Morillo, Jorge A., *A Fully Three-Dimensional Unsteady Rotor Inflow Model from a Galerkin Approach,* Doctor of Science Dissertation, Washington University, December 2001.

[17]Peters, David A. and Nelson, Adria M., "A Two-Dimensional Rotor Inflow Model Developed in Closed Form from a Galerkin Approach," Proceedings of the 18th AIAA Applied Aerodynamics Conference, Denver, Colorado, August 14-17, 2000.

[18]Peters, David A. and Nelson, Adria M., "A Two-Dimensional Rotor Inflow Model Developed in Closed Form from a Galerkin Approach," Proceedings of the American Helicopter Society Aeromechanics Specialists' Meeting, Atlanta, Georgia, November 13–14, 2000.

Appendix: Closed-Form Expressions

Mass Matrix

$$M_{jn}^{rm} = \frac{2}{\sqrt{H_n^m H_j^m}} \frac{(-1)^{\frac{n+j-2m}{2}} \sqrt{(2n+1)(2j+1)}}{(n+j)(n+j+2)\left[(n-j)^2-1\right]}$$

$$r = m; \quad j+r = odd; \quad n+m = odd \tag{A1}$$

$$M_{jn}^{rm} = \frac{1}{\sqrt{H_n^m H_j^r}\sqrt{(2n+1)(2j+1)}}$$

$$r = m; \quad j = n \pm 1; \quad j+r = odd; \quad n+m = even$$
$$r = m; \quad j = n \pm 1; \quad j+r = even; \quad n+m = odd \tag{A2}$$

$$M_{jn}^{rm} = \frac{8}{\pi^2\sqrt{H_n^m H_j^m}} \frac{(-1)^{\frac{n+j-2m+2}{2}} \sqrt{(2n+1)(2j+1)}}{(n+j)(n+j+2)\left[(n-j)^2-1\right]}$$

$$r = m; \quad j+r = even; \quad n+m = even \tag{A3}$$

$$M_{jn}^{rm} = 0$$

$$r \neq m \tag{A4}$$

Damping Matrix

$$D_{jn}^{rm} = \frac{1}{K_n^m}\delta_{jn}$$

$$r = m; \quad j+r = odd; \quad n+m = odd$$
$$r = m; \quad j+r = even; \quad n+m = even \tag{A5}$$

$$D_{jn}^{rm} = \frac{2}{\pi\sqrt{H_n^m H_j^m}} \frac{\sqrt{(2j+1)(2n+1)}}{(j+n+1)(j-n)} (-1)^{\frac{j+3n-1}{2}}$$

$$r = m; \quad j+r = odd; \quad n+m = even$$
$$r = m; \quad j+r = even; \quad n+m = odd \tag{A6}$$

$$D_{jn}^{rm} = 0$$

$$r \neq m \tag{A7}$$

Influence Coefficient Matrix

$$\left(\tilde{L}_{jn}^{0m^c}\right) = X^m \left(\Gamma_{jn}^{0m}\right) \tag{A8}$$

$$\left(\tilde{L}_{jn}^{rm^c}\right) = \left(X^{|m-r|} + (-1)^l X^{|m+r|}\right)\left(\Gamma_{jn}^{rm}\right) \tag{A9}$$

$$\left(\tilde{L}_{jn}^{rm^s}\right) = \left(X^{|m-r|} - (-1)^l X^{|m+r|}\right)\left(\Gamma_{jn}^{rm}\right) \tag{A10}$$

where

$$X = tan\left(\frac{\chi}{2}\right), \; l = min(r,m) \tag{A11}$$

$$\Gamma_{jn}^{rm} = \frac{sign(r-m)}{\sqrt{K_n^m K_j^r}\sqrt{(2n+1)(2j+1)}}\delta_{j,n\pm1}$$

$$r+m = odd; \; j+r = odd; \; n+m = odd \tag{A12}$$

$$\Gamma_{jn}^{rm} = \frac{(-1)^{\frac{n+j-2r}{2}}(2)\sqrt{(2n+1)(2j+1)}}{\sqrt{H_n^m H_j^r}(n+j)(n+j+2)\left[(n-j)^2-1\right]}$$

$$r+m = even; \; j+r = odd; \; n+m = odd \tag{A13}$$

$$\Gamma_{jn}^{rm} = \frac{(-1)^{\frac{n+j-2r+2}{2}}(8)\sqrt{(2n+1)(2j+1)}}{\pi^2\sqrt{H_n^m H_j^r}(n+j)(n+j+2)\left[(n-j)^2-1\right]}$$

$$r+m = even; \; j+r = even; \; n+m = even \tag{A14}$$

$$\Gamma_{jn}^{rm} = \frac{(-1)^{\frac{3n+j+2m-2r}{2}}(4)sign(r-m)\sqrt{(2n+1)(2j+1)}}{\pi\sqrt{H_n^m H_j^r}(n+j)(n+j+2)\left[(n-j)^2-1\right]}$$

$$r+m = odd; \; j+r = odd; \; n+m = even$$
$$r+m = odd; \; j+r = even; \; n+m = odd \tag{A15}$$

$$\Gamma_{jn}^{rm} = \frac{1}{\sqrt{H_n^m H_j^r}\sqrt{(2n+1)(2j+1)}}\delta_{j,n\pm1}$$

$$r+m = even; \; j+r = odd; \; n+m = even$$
$$r+m = even; \; j+r = even; \; n+m = odd \tag{A16}$$

$$K_n^m = \left(\frac{\pi}{2}\right)^{(-1)^{n+m}} H_n^m \tag{A17}$$

$$H_n^m = \frac{(n+m-1)!!(n-m-1)!!}{(n+m)!!(n-m)!!} \tag{A18}$$

1, 2, 3, 4, 5, 6, 7, 8, 9, 10, 11, 12, 13, 14, 15, 16, 17, 18,